Water Resources and Industry 30 (2023) 100226

Contents lists available at ScienceDirect

Water Resources and Industry

journal homepage: www.elsevier.com/locate/wri

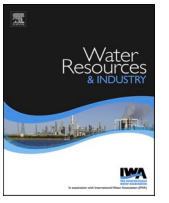

Bimetallic Bi/Cu^0-catalyzed persulfate-based advanced oxidation processes towards clofibric acid degradation in wastewater

Jibran Iqbal [a,*], Noor S. Shah [b,**], Javed Ali Khan [c], Mohamed A. Habila [d], Grzegorz Boczkaj [e,f], Asam Shad [g], Yousef Nazzal [h], Ahmed A. Al-Taani [h,i], Fares Howari [j]

[a] College of Interdisciplinary Studies, Zayed University, P.O. Box 144534, Abu Dhabi, United Arab Emirates
[b] Department of Environmental Sciences, COMSATS University Islamabad, Vehari Campus, 61100, Pakistan
[c] Department of Chemistry, Abdul Wali Khan University Mardan, Mardan, 23200, Pakistan
[d] Department of Chemistry, College of Science, King Saud University, P. O. Box 2455, Riyadh, 11451, Saudi Arabia
[e] Gdańsk University of Technology, Faculty of Civil and Environmental Engineering, Department of Sanitary Engineering, G. Narutowicza 11/12 Str, 80-233, Gdańsk, Poland
[f] EkoTech Center, Gdansk University of Technology, G. Narutowicza St. 11/12, 80-233, Gdansk, Poland
[g] Department of Environmental Sciences, COMSATS University Islamabad, Abbottabad Campus, Pakistan
[h] College of Natural and Health Sciences, Zayed University, P.O. Box 144534, Abu Dhabi, United Arab Emirates
[i] Department of Earth and Environmental Sciences, Faculty of Science, Yarmouk University, Irbid, Jordan
[j] College of Arts and Sciences, Fort Valley State University, Fort Valley, GA, 31030, USA

ARTICLE INFO

Keywords:
Pharmaceuticals
Contaminants of emerging concern
Bimetallic zerovalent metals
Advanced oxidation processes
Water treatment
Ecotoxicity investigation

ABSTRACT

Clofibric acid (CFA), an important blood-lipid regulatory drug is an emerging organic pollutant and widely reported in water resources. A novel bimetallic, bismuth/zero valent cupper (Bi/Cu^0) catalyst was prepared which showed better physiological, structural, and catalytic properties than Cu^0. The Bi/Cu^0 effectively catalyzed persulfate ($S_2O_8^{2-}$) and caused 85% degradation of CFA. The Bi coupling improved reusability and stability of Cu^0. The use of alcoholic and anionic radical scavengers and analyzing change in $[S_2O_8^{2-}]_0$ proved that Bi/Cu^0/$S_2O_8^{2-}$ yield hydroxyl radicals ($^{\bullet}OH$) and sulfate radicals ($SO_4^{\bullet-}$). The $^{\bullet}OH$ and $SO_4^{\bullet-}$ showed faster reaction with CFA, i.e., 4.65×10^9 and 3.82×10^9 M^{-1} s^{-1} and degraded CFA into four degradation products. Under optimal conditions of $[Bi/Cu^0]_0 = 1.0$ g/L and $[S_2O_8^{2-}]_0 = 40$ mg/L, 99.5% degradation of the 10 mg/L of CFA was achieved at 65 min. Temperature showed promising effects on the removal of CFA by Bi/Cu^0/$S_2O_8^{2-}$ and caused 98% removal at 323 K than 75% at 298 K at 32 min. The temperature effects were used to calculate activation energy, enthalpy, and rate constant of CFA degradation. The Bi/Cu^0/$S_2O_8^{2-}$ showed effective removal of CFA in real water samples also. The ecotoxicity study confirmed non-toxic product formation which suggests high capability of the proposed technology in the treatment of CFA.

* Corresponding author.
** Corresponding author.
E-mail addresses: Jibran.iqbal@zu.ac.ae (J. Iqbal), samadchemistry@gmail.com (N.S. Shah).

https://doi.org/10.1016/j.wri.2023.100226
Received 27 April 2023; Received in revised form 7 August 2023; Accepted 12 September 2023
Available online 15 September 2023

1. Introduction

Water is a fundamental component of life and used in many sectors, i.e., as a precursor of industrial products, cooling, transportation, agriculture, constructions, and energy production etc. [1,2]. The rapid pollution of water resources by different pollutants lead to increase stress on the available freshwater resources [3–5]. The different water pollutants include heavy metals, dyes, pesticides, and pharmaceutical products [6–12]. Pharmaceuticals products which are produced and used in large quantities contribute greatly into water pollution [13–17]. The pharmaceutical products and their metabolites are detected at lower concentrations in aquatic environment, however, their continuous discharge pose serious health and environment issues [13,14,18,19]. The pharmaceuticals are classified into different types in accordance with their functions, such as blood-lipid regulators, antibiotics, analgesic, and steroids etc. [13,14,20–22]. The pharmaceutical, clofibric acid (CFA, (*p*-Chlorophenoxy)-2-methylpropionic acid, $C_{10}H_{11}ClO_3$) is an important and active component of blood-lipid regulatory drugs. The CFA is widely used as a medication and reported to greatly contaminate aquatic environment [20,21,23]. The CFA is found to be highly persistent and causes endocrine disruption and numerous other health and environmental disturbances [20,21,23–25]. The ubiquitous presence in aquatic environment and greater toxicity, high persistency, and complex structure makes the use of conventional treatment technologies less effective in the treatment of CFA [22,24]. The CFA due to its high toxicity and persistency is resistant to biodegradation [22]. Adsorption technologies which involve only changing the physical form of the pollutant is also disfavored in treating CFA [22].

Alternatively, advanced oxidation processes (AOPs) which produces hydroxyl radical ($^{\bullet}OH$) and sulfate radical ($SO_4^{\bullet-}$) and effectively degrade toxic organic pollutants are receiving interests [11,26–30]. The activated persulfate (PS, $S_2O_8^{2-}$) is used as the source of $^{\bullet}OH$ and $SO_4^{\bullet-}$. Among the different activators, zerovalent metals, such as zerovalent copper (ZVCu, Cu^0) consistently provide metal ion for activating $S_2O_8^{2-}$ into $^{\bullet}OH$ and $SO_4^{\bullet-}$ and are preferably used (reaction (1) to (8)) [29,31–33]. Besides, the zerovalent metal-based activation process is recyclable as the metal ion is regenerated as shown in reaction (8). Contrary, in the metal ion activation of $S_2O_8^{2-}$, the metal ion need to be supplied continuously and could not be recycled [34].

$$2Cu^0 + 2H_2O \rightarrow 2Cu^+ + 2OH^- + H_2 \quad (1)$$

$$2Cu^+ + 2H_2O \rightarrow 2Cu^{2+} + 2OH^- + H_2 \quad (2)$$

$$2Cu^0 + S_2O_8{}^{2-} \rightarrow Cu^+ + H^+ + 2SO_4{}^{2-} \quad (3)$$

$$Cu^+ + S_2O_8{}^{2-} \rightarrow Cu^{2+} + SO_4{}^{2-} + SO_4{}^{\bullet-} \quad (4)$$

$$Cu^{2+} + S_2O_8{}^{2-} \rightarrow Cu^+ + S_2O_8{}^{\bullet-} \quad (5)$$

$$SO_4{}^{\bullet-} + H_2O \rightarrow SO_4{}^{2-} + {}^{\bullet}OH + H^+ \quad (6)$$

$$SO_4^{\bullet-} + {}^{-}OH \rightarrow SO_4^{2-} + {}^{\bullet}OH \quad (7)$$

$$Cu^0 + Cu^{2+} \rightarrow Cu^+ \quad (8)$$

The zerovalent metals, e.g., Cu^0 possess distinctive properties, e.g., low cost, high redox potential, greater recovery, high surface reactivity, and multiple treatment mechanisms [14,35–39]. These distinctive properties prefer the use of Cu^0 for activation of $S_2O_8^{2-}$ and treatment of large number of different organic and inorganic water contaminants [14,35–37]. However, bare Cu^0 is likely to undergo agglomeration, formation of passive layer, and leaching of metal ion which consequently could influence the formation of reactive radicals and treatment of contaminants [14]. These flaws are controlled by coupling Cu^0 with bismuth metal (Bi) andform bimetallic Bi/Cu^0. The Bi possess exceptional properties and reported in previous studies to pose significant impacts on improving distinct properties and catalytic activity of zerovalent metals [40–42].

This study was aimed to improve the physiological characteristics, reusability, stability, and catalytic activity of Cu^0 by coupling it with Bi. The prompt reactivity of bimetallic Bi/Cu^0 was suggested to accelerate the decomposition of $S_2O_8^{2-}$ into $^{\bullet}OH$ and $SO_4^{\bullet-}$. and degradation of CFA. Different studies were performed to assess the impacts of Bi on the reactivity and stability of Cu^0, yield of $^{\bullet}OH$ and $SO_4^{\bullet-}$, and degradation of CFA. The study of competition kinetic was used to calculate rate constants of $^{\bullet}OH$ and $SO_4^{\bullet-}$ with CFA. The oxidative degradation products of CFA were determined by mass spectrometric analysis to identify participation of $^{\bullet}OH$ and $SO_4^{\bullet-}$ into degradation of CFA. Other objectives of this study were to investigate the effects of different $[CFA]_0$, $[S_2O_8^{2-}]_0$, and $[Bi/Cu^0]_0$, different pH, inorganic ions, and temperature to optimize the treatment conditions. The effect of temperature was used to study different thermodynamic parameters, e.g., entropy and enthalpy of the treatment of CFA. The copper ion leaching into solution and cyclic treatment of CFA was done to investigate stability and reusability of the prepared materials. The Bi/Cu^0 was employed to treat CFA in real water samples with an aim to extend its potential practical applications. Besides, toxicities of CIP and its DPs, kinetics of degradation, and proposed degradation pathways were studied.

2. Material and method

2.1. Materials

CFA ($C_{10}H_{11}ClO_3$, 99%), sodium persulfate ($Na_2S_2O_8$, 98%), copper sulfate pentahydrate ($CuSO_5$,$5H_2O$, 98%), para-chlorobenzoic acid (*p*-CBA, 99%), meta-toluic acid (*m*-TA. 99%), and sodium borohydride (98%) were bought from Sigma-Aldrich. Other chemicals that include bismuth nitrate, perchloric acid ($HClO_4$), sodium hydroxide (NaOH), ethanol, *tert*-butyl alcohol (TBA), isopropyl alcohol (IPA), potassium chloride (KCl), sodium nitrite ($NaNO_2$), sodium carbonate (Na_2CO_3) and sodium bicarbonate ($NaHCO_3$), sodium nitrate ($NaNO_3$), cuprous chloride (CuCl), zinc nitrate ($Zn(NO_3)_2$), ferric chloride ($FeCl_3$), bismuth nitrate ($Bi(NO_3)_3$), ferrous sulfate ($FeSO_4$), and manganese chloride ($MnCl_2$) were purchased from Daejung, Korea. High purity deionized water (DI) prepared in the laboratory was used for preparing reaction solution.

2.2. Synthesis of zerovalent Bi/Cu^0 and Cu^0

The synthesis of Cu^0 was carried out by a simple titration method against the reductant, borohydride (BH_4^-) as presented in reaction (9).

$$Cu^{2+} + 2BH_4^- + 6H_2O \rightarrow Cu^0 + 2B(OH)_3 + 7H_2 \quad (9)$$

In the synthesis of Cu^0, the reaction solutions used were $CuSO_5$,$5H_2O$ (titrate) and sodium borohydride (titrant). Two 250 mL airtight conical flask were taken and used to prepare copper sulfate ($CuSO_4$) and sodium borohydride ($NaBH_4$) solutions separately. The copper sulfate solution (70 mL) was made by dissolving 4.0 g of copper sulfate in DI water and ethanol mixture (60:10). Ethanol was added to minimize access of air into the solution. Further, the copper solution was purged with N_2 gas for 20 min to eliminate any dissolved oxygen. The borohydride solution was prepared by dissolving 3.0 g of $NaBH_4$ in 80 mL DI water and transferred into burette for titrating copper solution. The $NaBH_4$ solution was started to add drop-wise into the copper solution which resulted into simultaneous formation of Cu^0 precipitate. The precipitate of Cu^0 was transferred to petri-dish and dried in oven at 65 °C for 7 h. The dried materials were kept in N_2 gas purged airtight glass vial.

The synthesis of Bi/Cu^0 was prepared by the same procedure used for Cu^0, except added 2.0 g bismuth nitrate (Bi precursor) with $CuSO_5$,$5H_2O$ and titrated the mixture of Bi and Cu solutions with borohydride. The precipitate of Bi/Cu^0 was transferred to petri-dish and dried in oven at 80 °C for 7 h.

2.3. Characterization

Different instruments were used to study the surface, structural, morphological, elemental characteristics as well as thermal stability of the Cu^0 and Bi/Cu^0. Scanning electron microscope and x-ray electron spectroscopy (SEM-EDX, TESCAN VEGA (LMU)/SEM), INCAx-act (Oxford Instruments)/EDX) instruments were utilized to identify morphology of Cu^0 and Bi/Cu^0 and dispersion of different elements on their surfaces. The identification of different functional groups in the prepared Cu^0 and Bi/Cu^0 was performed by Fourier transform infra-red spectrophotometer (FTIR, Thermo Scientific/Nicolet-6700TM). The crystallographic and thermal characteristics of the Cu^0 and Bi/Cu^0 were identified by x-ray diffractometer (XRD/Rigaku Ultima III) and thermal gravimetric analyzer (TGA/PerkinElmer/STA 6000), respectively.

2.4. Catalytic performance of Cu^0 and Bi/Cu^0 and analysis of CFA

The catalytic activities of Cu^0 and Bi/Cu^0 were investigated in the absence and presence of $S_2O_8^{2-}$ using CFA as the target contaminant. A 100 mL of CFA solution was prepared in airtight conical flask using 10 mg/L of $[CFA]_0$, 500 mg/L of $[Cu^0]_0$ and $[Bi/Cu^0]_0$, and 80 mg/L of $[S_2O_8^{2-}]_0$ and treated for 0–65 min using stirring. A 250 μL of solution was taken at each treatment interval and analyzed with high performance liquid chromatography (HPLC, Agilent Technologies/1200 Series) using quaternary pump. A C18 column (XDB, particle size 5 μm, 150 × 4.6 mm (i.d.)) and a UV–Vis detector fixed at 230 nm wavelength was used for analysis. Acetonitrile/0.05 M oxalic acid (40: 60) mixture (isocratic mode) was used as a mobile phase (at 1.0 mL/min flow rate). From the treated solution, 20 μL of sample was injected into the HPLC.

Gas-chromatography/mass spectrometry (GC/MS, Agilent-8890/5977) was used to determine degradation products of CFA. The carrier gas was helium (purity 99.99%) and the capillary column (30 m, internal diameter 0.25 μm) was HP-5 (5%-phenyl methyl siloxane). The injector was set at 250 °C and in splitless mode while oven temperature programmed as: 60 °C (hold for 4 min) and increased to 160 °C at a ramp rate of 10 °C/min (hold for 2 min) and finally increased to 250 °C at 10 °C/min (hold for 7 min).

For pH studies, a 0.05 M of $HClO_4$ or NaOH was added for adjusting desired pH. The lower reactivity of ClO_4^- with $^{\bullet}OH$ and $SO_4^{\bullet-}$ prefer using $HClO_4$.

The effects of the process parameters, e.g., initial concentrations of CFA, Cu^0, and $S_2O_8^{2-}$, and inorganic ions (anions and cations) were checked in separate experiments using each of these species. The hot plat magnetic stirrer was used for treatment of CFA at different temperatures (T), i.e., 298, 303, 313, and 323 K. The temperature effect was used to calculate thermodynamic parameters, e.g., activation energy (Ea) and enthalpy of (ΔH) of CFA treatment using Arrhenius equations (equation (10)) and transition state theory (equation (11)), respectively.

$$-\ln k_{obs} = \frac{Ea}{RT} - \ln A \tag{10}$$

$$\Delta H = Ea - RT \tag{11}$$

In the above equations, A is Arrhenius constant, R is gas constant = 8.31 J/mol/K and k_{obs} is observed degradation constant.

The change in $[S_2O_8^{2-}]_0$ was checked according to the procedure described by Liang et al. [43] calorimetric method to reveal decomposition of $S_2O_8^{2-}$ into reactive radicals. The competition kinetic studies were performed in the presence of *p*-CBA and *m*-TA to measure rate constants of CFA with $^{\bullet}OH$ and $SO_4^{\bullet-}$ which is discussed in detail our previous study [39,44]. The competitors, *p*-CBA and *m*-TA were used at identical concentration as CFA and analyzed by HPLC method from He et al. [45] study.

For studying reusability, the prepared Cu^0 and Bi/Cu^0 were separated from treated solution, washed three times with water using centrifuge and reused for treatment of the target pollutant. The level of leached Cu ions in treated solutions at each cycle was monitored by atomic absorption spectrophotometry at 324.8 nm wavelength.

The CFA was treated in two real water samples collected from Canal View Vehari (Sample 1) and Sharqi Colony Vehari (Sample 2). The physical and chemical properties of these real water samples are presented in our published study [28].

2.5. Ecotoxicological study

For identifying the ecotoxicological effects of CFA and its products, the computerized structural-based toxicity evaluation program, ECOSAR (Ecological Structure Activity Relationship) was used. ECOSAR was used to identify acute and chronic toxicities toward three different aquatic organisms, fish, daphnia, and green algae [46]. The acute toxicities denoted as LC_{50} and EC_{50} were monitored by short- or long-time exposure of organisms to chemicals while chronic toxicities denoted as ChV were determined from long-term exposure to chemicals [47,48]. The LC_{50} depicts the chemicals level that can stop growth of 50% daphnia and fish after 48 and 96 h exposure times, respectively. On contrary, EC_{50} depict the level of toxin that can decline 50% green algae growth after 96 h exposure time [47,48].

3. Results and discussions

3.1. Structural characteristics of Bi/Cu^0 and Cu^0

The data obtained from IR analysis of Cu^0 and Bi/Cu^0 (in the 4000 to 400 cm^{-1} wavelength range) is shown in Fig. 1a. The bands at 670 and 1150–1270 cm^{-1} were ascribed to Cu–O and C–O stretching vibrations, respectively. The spectra showed band at 960 cm^{-1} which was ascribed to B–O bonds in v1 (BO_3) and found to arise due to reducing agent, BH_4^- [39]. In addition, spectra of Bi/Cu^0 showed bands at 500 and 1000 cm^{-1} due to Bi–O bonds and suggest Bi pairing with Cu^0 [49]. In the IR spectra, the band observed at 3300 cm^{-1} was assigned to O–H stretching vibration.

The data obtained from XRD analysis of Cu^0 and Bi/Cu^0 (at 2θ degree range of 10–80) is presented in Fig. 1b. The XRD graph

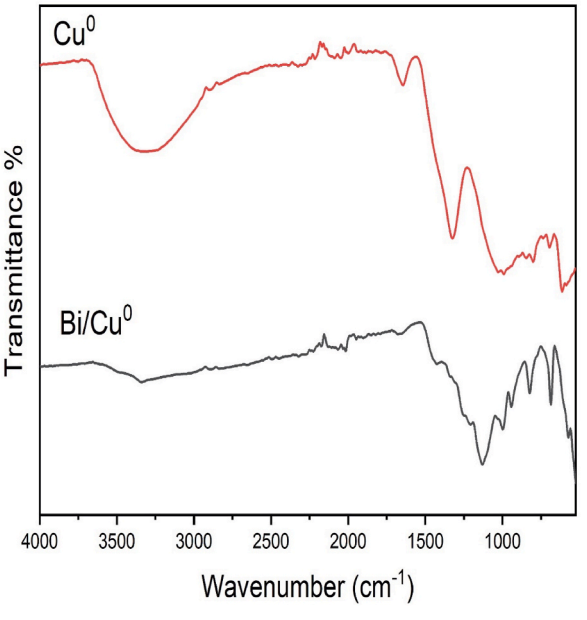

Fig. 1a. FTIR analysis spectra of Cu^0 and Bi/Cu^0.

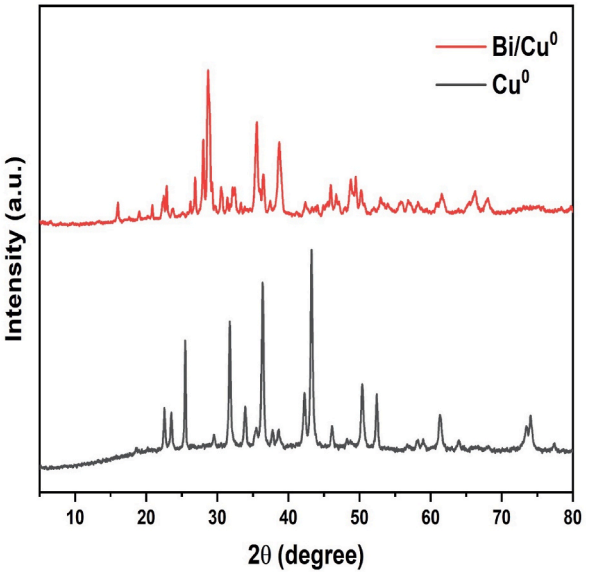

Fig. 1b. Graph of the XRD analysis of Cu^0 and Bi/Cu^0.

showed peaks at 2θ of 37, 43 and 50.5° due to Cu^0 (JCPDS 89–2838)). The peaks found at 43 and 50.5° signifies the (111) and (200) planes of Cu^0. The Cu^0 peaks identified in XRD analysis suggest successful formation of Cu^0 and Bi/Cu^0. The XRD data showed peaks at 2 theta values of 35.5, 62.5, and 73.5° which were ascribed to Cu_2O. The Bi/Cu^0 crystal showed one peak of Cu_2O which suggest inhibited corrosion of Cu^0 by Bi. Contrary to Cu^0, XRD data of Bi/Cu0 showed peak of Bi at a 2θ of 27.5 which portrayed successful Bi coupling with Cu^0 and formation of Bi/Cu^0 [41]. This XRD data was used to calculate the degree of crystallinity (DOC%) and crystallite size (D) of the Cu^0 and Bi/Cu^0 using the following equations (12) and (13) [5,13,50].

$$DOC\% = \frac{A_c - A_a}{A_c} \times 100 \tag{12}$$

$$D = \frac{K\lambda}{\beta\, Cos\, \theta} \tag{13}$$

In equation (12), the total area under crystalline phase (Ac) and amorphous phase (Aa) were measured and DOC% was calculated as 72 and 74 for Cu^0 and Bi/Cu^0, respectively. The Scherrer equation (13) was used to calculate the crystallite size D (nm) using the values of $K = 0.89$, $\lambda = 0.154$ nm, $\beta =$ difference in 2θ at half maximum, and cos of θ. The D values for Cu^0 and Bi/Cu^0 were calculated as 3.6 and 3.1 nm respectively. The high degree of crystallinity and small crystallite size suggest high catalytic activity of Bi/Cu^0 than Cu^0 [51].

Fig. 1c depicts the morphological characteristics of Cu^0 and Bi/Cu^0obtained from SEM analysis. The Cu^0 particles showed highly agglomerated hollow channels consisting of porous layers (Fig. 1c (A)). However, the SEM result showed particle of Bi/Cu^0 to be less agglomerated and rough clusters with irregular quasi-spherical geometry (Fig. 1c (B)). The less agglomerated structure of Bi/Cu^0 could be due to the coupled Bi. Further, the presence of coupled Bi and formation of bimetallic Bi/Cu^0 was determined by EDX analysis. The EDX results of Cu^0 and Bi/Cu^0 are presented in Fig. 1d (A) and 1d (B), respectively. The elemental composition from EDX analysis of

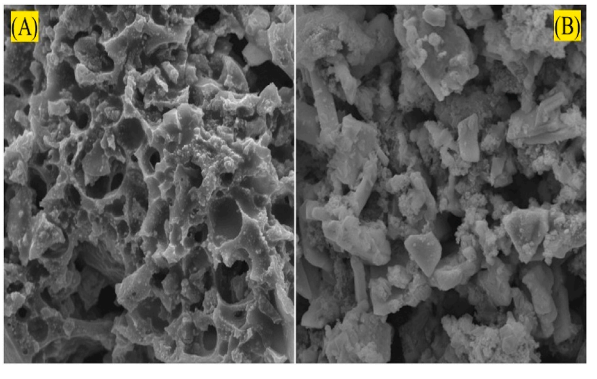

Fig. 1c. SEM micrograph of (A) Cu^0 and (B) Bi/Cu^0.

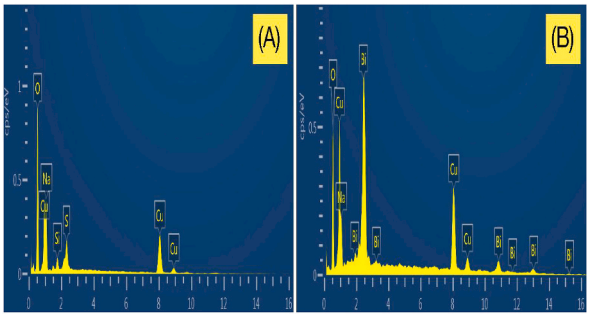

Fig. 1d. EDX spectra of (A) Cu^0 and (B) Bi/Cu^0.

Cu^0 given in Fig. 1d (A) depict the presence of Cu, S, Na, and O peaks. On contrary, the EDX analysis of BI/Cu^0 depict the presence of Cu, Bi, O, and Na peaks (Fig. 1d (B)). The Cu peaks in the EDX spectra of both Cu^0 and BI/Cu^0 illustrate successful formation of zerovalent copper by the borohydride-based reduction method. The N and S peaks looked to arise from the sodium borohydride and copper sulfate salts used as precursor salts. The Bi peak found only in Bi/Cu^0 depicts successful coupling of Bi with Cu^0.

Results from thermogravimetric analyses of Cu^0 and BI/Cu^0 are shown in Fig. 1e which illustrate high weight (%) loss to heat treatment in Cu^0 than Bi/Cu^0 till 690 °C. The weight (%) loss was sharp initially in both Cu^0 and Bi/Cu^0 possibly due to the loss of adsorbed moisture and water on the surface of the catalysts. At later stage, the Cu^0 showed a dramatic increase in the weigh (%) loss which is reported due to oxidation of the bare zerovalent metal at later stage of heat treatment [42].

3.2. Catalytic degradation of CFA

The activities of Cu^0 and Bi/Cu^0 combined with $S_2O_8^{2-}$ were checked for degradation of CFA and compared the results with control experiments using only $S_2O_8^{2-}$, Cu^0, and Bi/Cu^0. The results obtained are presented in Fig. 2 which showed 9, 36, 50, 67, and 85% loss of CFA by $S_2O_8^{2-}$, Cu^0, Bi/Cu^0, $Cu^0/S_2O_8^{2-}$, and $Bi/Cu^0/S_2O_8^{2-}$, respectively, at 65 min. The high CFA removal by the Cu^0 and Bi/Cu^0-catalyzed $S_2O_8^{2-}$ process could be due to the $^{\bullet}OH$ and $SO_4^{\bullet-}$ formed as shown in reactions (1) to (7). It is found that Cu metal loss electrons which are taken by $S_2O_8^{2-}$ and decomposed into $^{\bullet}OH$ and $SO_4^{\bullet-}$ (reactions 3 to 4) [28,29,39,52]. The $^{\bullet}OH$ and $SO_4^{\bullet-}$ quickly react with CFA and initiate its degradation into products. In the case of Bi/Cu^0, the coupled Bi form Bi–Cu bond which facilitate transfer of electron to $S_2O_8^{2-}$ and possibly increase the formation rate of $^{\bullet}OH$ and $SO_4^{\bullet-}$ [53,54]. This rapid formation of $^{\bullet}OH$ and $SO_4^{\bullet-}$ consequently trigger higher CFA degradation in Bi/Cu^0 than Cu^0. In addition, in Bi/Cu^0, both metals could cause decomposition of $S_2O_8^{2-}$. Other possibility looked that the coupled Bi could increase surface area of Bi/Cu^0 and accommodate more $S_2O_8^{2-}$ and CFA than only Cu^0. Besides, in bimetallic zerovalent metals, the second metal is reported to prevent corrosion and improve surface roughness which looked as the possible reasons for high performance of Bi/Cu^0 than Cu^0 [55]. The considerable removal of CFA by Cu^0 and Bi/Cu^0 alone could be due to adsorption of CFA and reduction reactions (due to loss of electrons) [39,56]. The zerovalent metals are

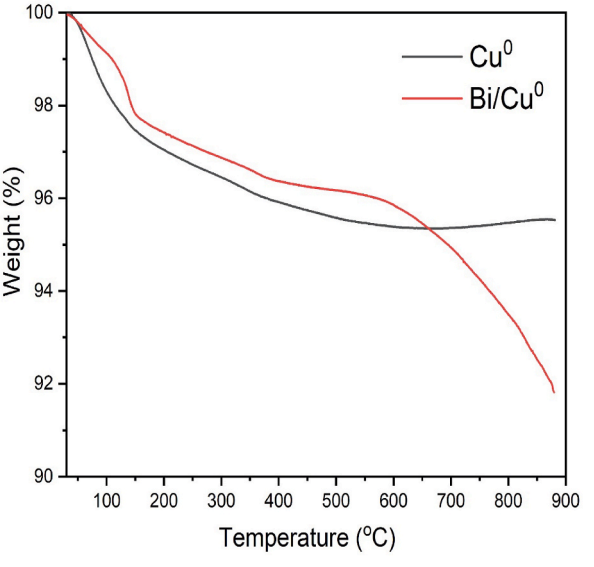

Fig. 1e. Graph of the TGA analysis of Cu^0 and Bi/Cu^0.

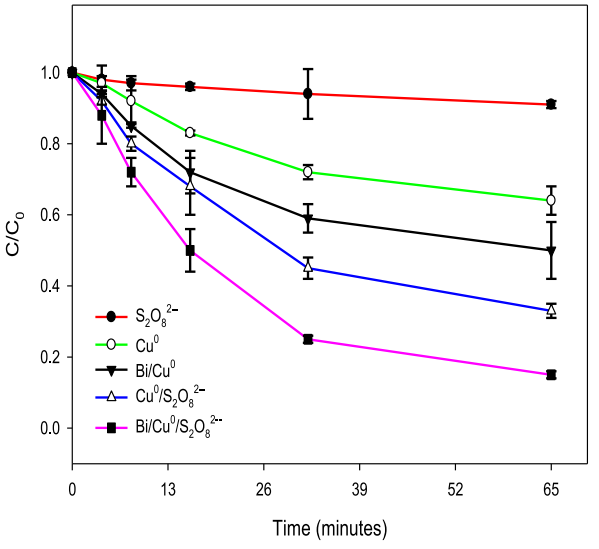

Fig. 2. Treatment of CFA by $S_2O_8^{2-}$, Cu^0, Bi/Cu^0, $Cu^0/S_2O_8^{2-}$, and Bi/$Cu^0/S_2O_8^{2-}$ processes. $[CFA]_0 = 10$ mg/L, $[S_2O_8^{2-}]_0 = 40$ mg/L, $[Cu^0]_0 = [Bi/Cu^0] = 0.5$ g/L, pH = 5.6.

reported to be strong reductant and reportedly cause rapid dehalogenation of halogenated compounds, like CFA [39,56].

The reactions involving catalytic activation of $S_2O_8^{2-}$ into $^{\bullet}OH$ and $SO_4^{\bullet-}$ and degradation of CFA occur on the surface of the catalyst.

Different processes, e.g., competition kinetics, use of radical scavengers, and monitoring change in concentration of $S_2O_8^{2-}$ were performed to elucidate (1 $^{\bullet}OH$ and $SO_4^{\bullet-}$ formation from the Cu^0 and Bi/Cu^0-mediated $S_2O_8^{2-}$ processes and (2 contribution of $^{\bullet}OH$ and $SO_4^{\bullet-}$ in CFA degradation. The study of competition kinetics was used to calculate rate constants of $^{\bullet}OH$ and $SO_4^{\bullet-}$ with CFA using the method reported by Shah et al. [39]. The results obtained showed high-rate constants values of $^{\bullet}OH$ and $SO_4^{\bullet-}$ with CFA, e.g., $k_{^{\bullet}OH/CFA} = 4.65 \times 10^9$ and $k_{SO_4^{\bullet-}/CFA} = 3.82 \times 10^9$ L/mol/s. The study of radical scavenging was performed with iso-propyl alcohol (IPA) as both $^{\bullet}OH$ ($k_{^{\bullet}OH/IPA} = 1.9 \times 10^9$ L/mol/s) and $SO_4^{\bullet-}$ ($k_{SO_4^{\bullet-}/IPA} = 8.2 \times 10^7$ L/mol/s) scavenger while *tert*-butyl alcohol (TBA) for only $^{\bullet}OH$, i.e., ($k_{^{\bullet}OH/TBA} = 6.0 \times 10^8$ L/mol/s) scavenging. The removal of CFA by the IPA and TBA with Cu^0 and Bi/Cu^0-mediated $S_2O_8^{2-}$ processes, i.e., $Cu^0/S_2O_8^{2-}$/IPA, $Cu^0/S_2O_8^{2-}$/TBA, Bi/$Cu^0/S_2O_8^{2-}$/IPA, and Bi/$Cu^0/S_2O_8^{2-}$/TBA was obtained as 27, 37, 34, and 47%, respectively (Fig. 3). The diminished removal of CFA using IPA and TBA demonstrate that Cu^0-and Bi/Cu^0 catalyze $S_2O_8^{2-}$ into $^{\bullet}OH$ and $SO_4^{\bullet-}$ that subsequently facilitated CFA abatement. Further studies utilizing different concentrations of IPA and TBA, 100,

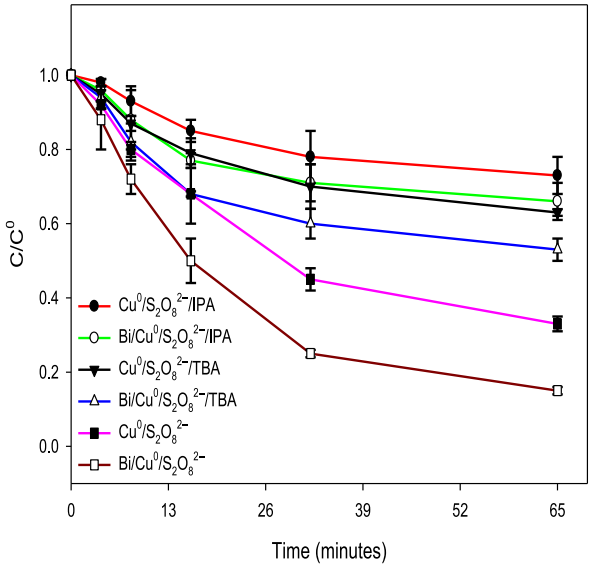

Fig. 3. Impacts of TBA and IPA on the activity off $Cu^0/S_2O_8^{2-}$ and Bi/$Cu^0/S_2O_8^{2-}$. $[CFA]_0 = 10$ mg/L, $[S_2O_8^{2-}]_0 = 40$ mg/L, $[Cu^0]_0 = [Bi/Cu^0] = 0.5$ g/L, $[TBA]_0 = [IPA] = 200$ mg/L, pH = 5.6.

200, 400, and 800 mg/L on the removal of CFA by $Cu^0/S_2O_8^{2-}$ and $Bi/Cu^0/S_2O_8^{2-}$ were investigated to accurately ensure the yield of $^{\bullet}OH$ and $SO_4^{\bullet-}$ and their contribution in the removal of CFA. The results obtained under these conditions are illustrated in Table 1 which show strong inhibition of CFA degradation efficiency at elevated level IPA and TBA. Reactivities depend on the product of second order rate constant and concentration, the use of high concentration of scavenger than CFA shift the probability of reaction of reactive radicals more towards scavengers [57].

The %decomposition as a function of change in initial concentrations of $S_2O_8^{2-}$ was calculated as 52 and 76% by Cu^0 and Bi/Cu^0 at 65 min, respectively (Data not shown). The high degree of %decomposition also illustrates Cu^0-and Bi/Cu^0-catalyzed $S_2O_8^{2-}$ reaction into $^{\bullet}OH$ and $SO_4^{\bullet-}$. The study by Wang et al. [33] utilizing radical scavengers and electron spin resonance (ESR) studies also revealed both $^{\bullet}OH$ and $SO_4^{\bullet-}$ formation in the zerovalent metal-mediated $S_2O_8^{2-}$ process.

Further experiments based on the analysis of oxidative degradation products of CFA by GC-MS analysis were carried out to elucidate initiation of CFA degradation by $^{\bullet}OH$ and $SO_4^{\bullet-}$. The Cu^0-and Bi/Cu^0-catalyze $S_2O_8^{2-}$ into $^{\bullet}OH$ and $SO_4^{\bullet-}$ (reactions (1) to (7)) and the latter cause oxidative degradation of CFA. In the present study, the reactions of $^{\bullet}OH$ and $SO_4^{\bullet-}$ gave four degradation products of CFA (Scheme 1). Due to identical pathways caused by $^{\bullet}OH$ and $SO_4^{\bullet-}$, the products found were ascribed to both radicals. The formation of 2-(4-hydroxyphenoxy)-isobutyric acid occurred through $^{\bullet}OH$ and $SO_4^{\bullet-}$ reaction at the C_4–Cl bond (enclosed in bracket) of CFA as given in reaction (14). The Cl group is substituted by OH group and form hydroxylated product (2-(4-hydroxyphenoxy)-isobutyric acid). This product is reported in previous AOPs-based degradation of CFA also [17,58]. The formation of 4-chlorphenol was produced due to reaction of $^{\bullet}OH$ and $SO_4^{\bullet-}$ at the C_1–O bond (reaction (15)) which subsequently undergo cleavage of C_1–O bond, hydrolysis and loss of 2-hydroxy isobutyric acid [17,25]. The product, chlorobenzene was formed by $^{\bullet}OH$ and $SO_4^{\bullet-}$ reactions at the C_1–O bond with subsequent loss of 2-hydroxy isobutyric acid (reaction (16)). The product identified as hydroquinone was found form the degradation of both 2-(4-hydroxyphenoxy)-isobutyric acid and 4-chlorphenol through the losses of 2-hydroxy isobutyric acid and chlorine group, respectively (reaction (17) and (18)). It has been stated in previous studies that these small intermediates are mineralized by $^{\bullet}OH$ and $SO_4^{\bullet-}$ into non-toxic organic acids, acetate etc. and even CO_2 and H_2O [17,29].

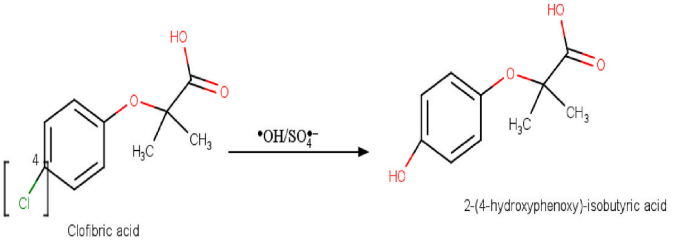

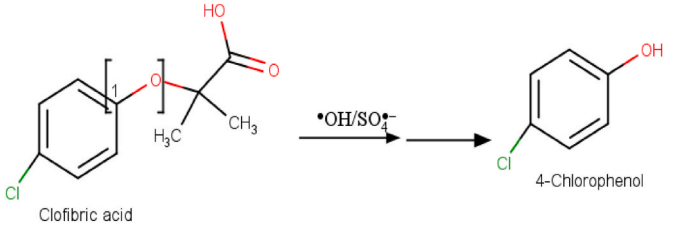

Table 1
Impacts of doses of IPA and TBA on degradation of CFA by $Cu^0/S_2O_8^{2-}$ and $Bi/Cu^0/S_2O_8^{2-}$. $[CFA]_0 = 10$ mg/L, $[S_2O_8^{2-}]_0 = 40$ mg/L, $[Cu^0]_0 = [Bi/Cu^0] = 0.5$ g/L, pH = 5.6.

Scavengers	Concentration of Scavengers (mg/L)	Removal efficiency (%)	
		$Cu^0/S_2O_8^{2-}$	$Bi/Cu^0/S_2O_8^{2-}$
IPA	800	5	9
	400	12	20
	200	27	34
	100	40	46
TBA^+	800	10	15
	400	22	35
	200	37	47
	100	46	59
No scavenger	–	67	85

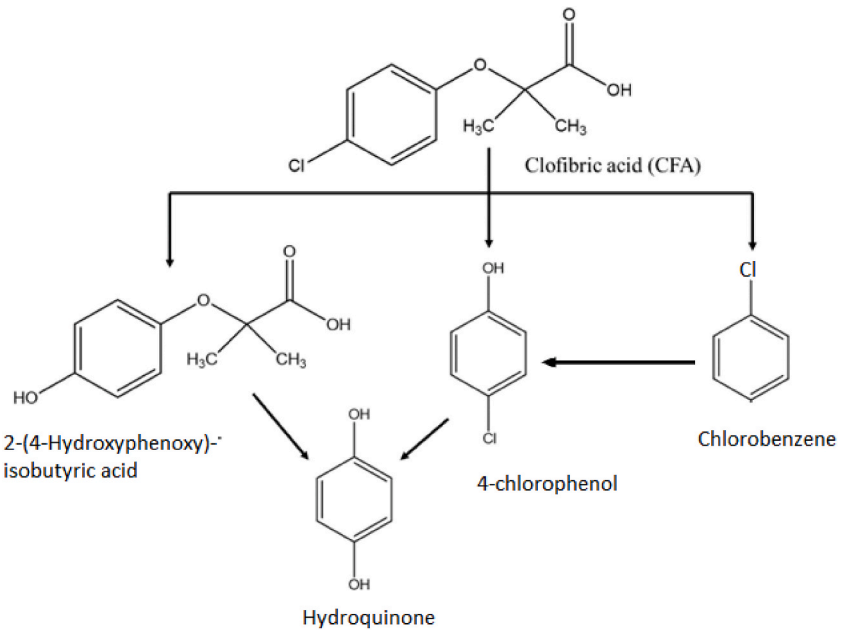

Scheme 1. Schematic presentation of $^{\bullet}OH$ and $SO_4^{\bullet-}$-based degradation pathways of clofibric acid.

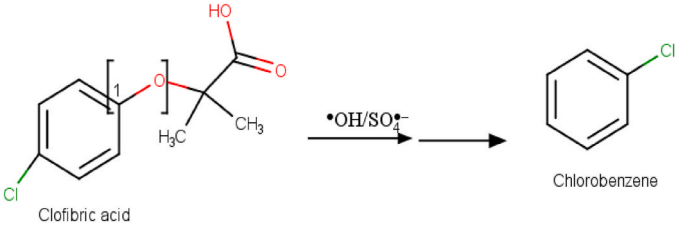

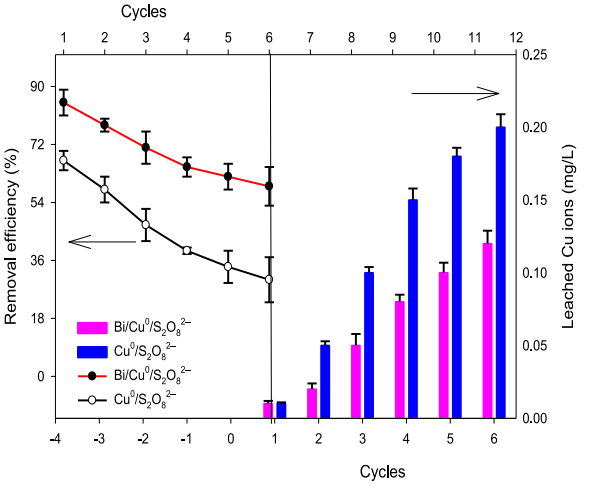

Fig. 4. Reusability efficiency and leaching of Cu ions analysis of the $Cu^0/S_2O_8^{2-}$ and $Bi/Cu^0/S_2O_8^{2-}$ processes: $[CFA]_0 = 10$ mg/L, $[S_2O_8^{2-}]_0 = 40$ mg/L, $[Cu^0]_0 = [Bi/Cu^0] = 0.5$ g/L, pH = 5.6.

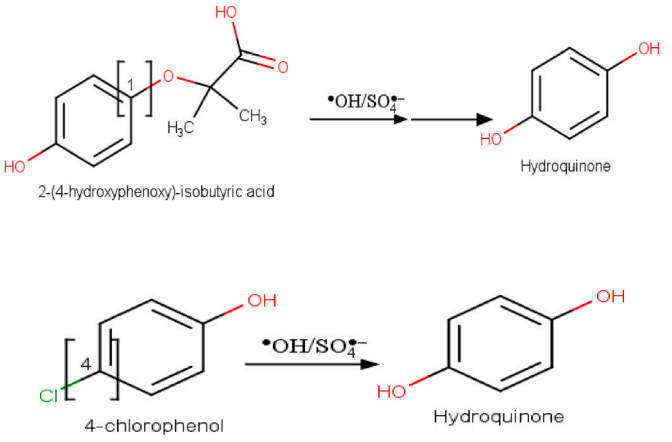

3.3. Reusability and leaching studies

Reusability and leaching of metal ions are key factors to evaluate practical applicability and environmentally friendly nature of any metallic nanoparticles. The reusability of Cu^0-and Bi/Cu^0-catalyzed $S_2O_8^{2-}$ process was assessed to degrade CFA for six consecutive cycles. The materials were recovered at each cycle and used for treating CFA in the presence of $S_2O_8^{2-}$. The degree of percent degradation was calculated at each cycle and given in Fig. 4. The percent degradation profile depict that Cu^0 and Bi/Cu^0 caused CFA degradation of 67 and 85% at first cycle while 30 and 58% at sixth cycle, respectively. These findings illustrate a drop of 55 and 30% in the performance of Cu^{0-} and Bi/Cu^0-catalyzed $S_2O_8^{2-}$ processes, respectively. The high %degradation achieved by Bi/Cu^0 at sixth cycle suggest its high reusability potential than Cu^0. The leaching of Cu ions in the Cu^0 and Bi/Cu^0-treated CFA solutions were analyzed to assess their stability. The level of leached Cu ions analyzed in the Cu^0 and Bi/Cu^0-treated solutions was found as 0.20 and 0.12 mg/L, respectively. The smaller level of Cu ions leaching observed in Bi/Cu^0 imply its substantial stability than Cu^0.

3.4. Influence of $S_2O_8^{2-}$ dosage on the CFA degradation

In this study, different dosages of $S_2O_8^{2-}$, i.e., 20, 40, and 80 mg/L were combined with Bi/Cu^0 (0.5 g/L) and applied for degradation of 10 mg/L of CFA. The results given in Fig. 5 display accelerated degradation of CFA at high dose of $S_2O_8^{2-}$ and vice versa. The degradation efficiency (%) of CFA was obtained to be 63, 85, and 98.4% at 20, 40, and 80 mg/L dosages of $S_2O_8^{2-}$, respectively. The same trend of synergistic role of high $[S_2O_8^{2-}]_0$ on degradation is witnessed in earlier studies [29,59,60]. The high dosages of $S_2O_8^{2-}$ increase its contact with the catalyst and consequently led to accelerated decomposition of $S_2O_8^{2-}$ into $^{\bullet}OH$ and $SO_4^{\bullet-}$ [60]. The accelerated formation of $^{\bullet}OH$ and $SO_4^{\bullet-}$ consequently led to their rapid collision with CFA molecules and cause high degree of CFA

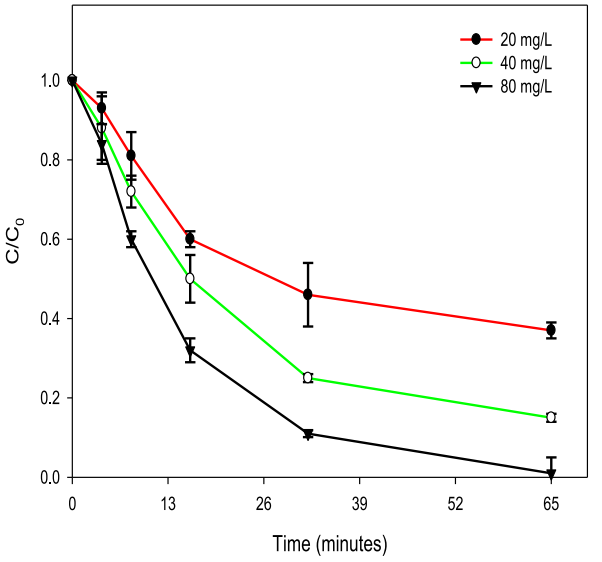

Fig. 5. Impacts of $[S_2O_8^{2-}]_0$ on the treatment of CFA by $Bi/Cu^0/S_2O_8^{2-}$. $[CFA]_0 = 10$ mg/L, $[S_2O_8^{2-}]_0 = 20$–80 mg/L, $[Bi/Cu^0] = 0.5$ g/L, pH = 5.6.

degradation. The kinetics of CFA degradation at different dosages of $S_2O_8^{2-}$ were investigated and found *pseudo-first-order* as presented in equation (19).

$$\frac{-d[CFA]}{dt} = k\,[CFA]_0 \tag{19}$$

The high dosage of $S_2O_8^{2-}$ resulted in high degradation rate constant, *k* which could be because of accelerated rate of $^{\bullet}OH$ and $SO_4^{\bullet-}$ formation and rapid collision of the later with CFA molecules.

3.5. Influence of dosages of Bi/Cu^0

Fig. 6 display the degradation pattern of CFA at different dosages of the catalyst, Bi/Cu^0 using fix concentrations of $S_2O_8^{2-}$ and CFA, e.g., 40 and 10 mg/L, respectively. The removal efficiency of CFA was 69, 85, and 99.5% for three different dosages of Bi/Cu^0, i.e., 0.25, 0.50, and 1.0 g/L, respectively, at 65 min. The catalyst accelerates $S_2O_8^{2-}$ into $^{\bullet}OH$ and $SO_4^{\bullet-}$ and the later initiate degradation of CFA, Thus, high dose of Bi/Cu^0 is expected to decompose $S_2O_8^{2-}$ violently and significantly accelerate yield of $^{\bullet}OH$ and $SO_4^{\bullet-}$. The accelerated formation of $^{\bullet}OH$ and $SO_4^{\bullet-}$ at high dosage of Bi/Cu^0 was monitored from change in concentration of $S_2O_8^{2-}$. The result (data not shown) showed synergetic effects of the dosage Bi/Cu^0 on the %decomposition of $S_2O_8^{2-}$.

The increasing level of Bi/Cu^0 could provide more space for the accumulation of CFA molecules and consequently led to high CFA removal at 1.0 g/L in our study. Besides, the high level of Bi/Cu^0 can accumulate maximum number of $S_2O_8^{2-}$ that consequently undergo rapid reactions with the catalyst and consequently rapidly decompose into $^{\bullet}OH$ and $SO_4^{\bullet-}$.

3.6. Influence of different operational parameters on CFA degradation

In this study, degradation of CFA by Bi/Cu^0-catalyzed $S_2O_8^{2-}$ based process was assessed under different conditions of $[CFA]_0$, pH of aqueous solutions, temperature, and commonly found inorganic ions in water. The purpose of these studies was to optimize the catalytic activity and potential of the Bi/Cu^0-catalyzed $S_2O_8^{2-}$ process for the treatment of CFA under different conditions.

Impact of initial CFA concentration: The change in concentrations of target contaminants is reported to exhibit different competition towards $^{\bullet}OH$ and $SO_4^{\bullet-}$ and adsorption sites [28,29,61]. As a result, different degradation efficiency of CFA is expected at different $[CFA]_0$ under fixed dosages of the catalyst and $S_2O_8^{2-}$. This phenomenon was studied by treating different concentrations of CFA, i.e., 5, 10, and 20 mg/L with Bi/Cu^0-catalyzed $S_2O_8^{2-}$ process. The results obtained are presented in Fig. 7a which showed non-linear relationship between $[CFA]_0$ and degradation efficiency. As discussed in section 3.2, the Bi/Cu^0-catalyzed $S_2O_8^{2-}$ degrade CFA into several degradation products which also reacts with $^{\bullet}OH$ and $SO_4^{\bullet-}$. Thus, the CFA undergo competition with its products for $^{\bullet}OH$ and $SO_4^{\bullet-}$ and rate of this competition increases with increasing target contaminant concentration [28,29]. At constant $[S_2O_8^{2-}]_0$, the high $[CFA]_0$ sink the ratio of $^{\bullet}OH$ and $SO_4^{\bullet-}$ to target contaminant molecules and subsequently decrease degradation efficiency of CFA [61]. Besides, degradation of high $[CFA]_0$ increase yield of degradation products and the later undergo high competition with parent compound for adsorption sites.

The kinetics of CFA degradation by Bi/Cu^0-catalyzed $S_2O_8^2$ was found to best fit *pseudo-first-order* kinetic. The *pseudo-first-order* degradation rate constants, *k* were estimated from equation (19) for different $[CFA]_0$ and exhibited decreasing trend with increasing $[CFA]_0$. The reasons for the low *k* at high $[CFA]_0$ are stated to be high degree of competition between CFA molecules and its products for $^{\bullet}OH$ and $SO_4^{\bullet-}$ and adsorption sites [28,29,61].

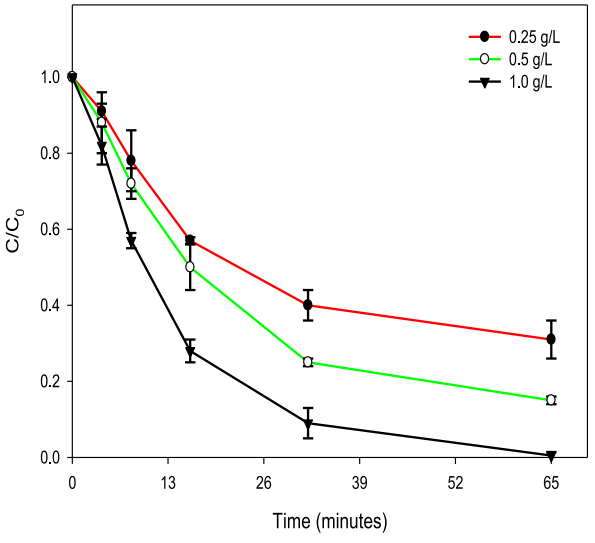

Fig. 6. Impacts of $[Bi/Cu^0]_0$ on the treatment of CFA by $Bi/Cu^0/S_2O_8^{2-}$. $[CFA]_0 = 10$ mg/L, $[S_2O_8^{2-}]_0 = 40$ mg/L, $[Bi/Cu^0] = 0.25$–1.0 g/L, pH = 5.6.

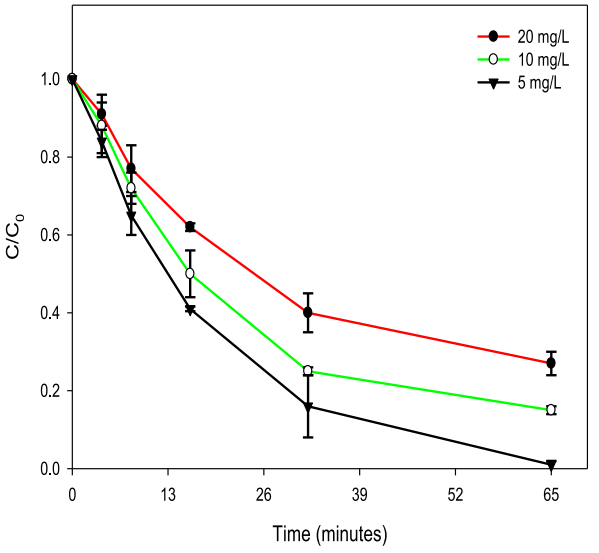

Fig. 7a. Impacts of $[CFA]_0$ on the treatment of CFA by $Bi/Cu^0/S_2O_8^{2-}$. $[CFA]_0$ = 5–20 mg/L, $[S_2O_8^{2-}]_0$ = 40 mg/L, $[Bi/Cu^0]$ = 0.25 g/L, pH = 5.6.

Impact of* pH *change: pH is an important parameter which influence catalytic activation of peroxides, yield of reactive radicals, and chemical nature of catalyst and target pollutant [62,63]. To look into these facts, the treatment of CFA by Bi/Cu^0-catalyzed $S_2O_8^{2-}$ process was investigated at different pH conditions, i.e., 2.5, 5.6, 8.5, and 10.6. The results presented in Fig. 7b depict high degree of CFA degradation at pH 5.6, i.e., 85% followed by 78, 56, and 25% at pH 2.5, 8.5, and 10.6, respectively. Zerovalent copper with a reported point-of-zero charge (PZC) as 8.2 suggest positive charge surface of Bi/Cu^0 at pH < 8.2 and negative charge at high pH than 8.2 [64]. The CFA which demonstrates pKa value of 3.18 exists in deprotonated form (negative charge) at pH > 3.18. However, it is reported to exist in molecular form at 2 < pH < 3.18 and acidic forms at a pH < 2 [65]. The trend of pKa and PZC values suggest high degree of attraction between CFA molecules and Bi/Cu^0 in the pH ranges of 3.18 < pH < 8.2 which subsequently led to high percentage of CFA degradation in this pH range. Besides, anionic form of CFA is reported to be highly reactive than its neutral and cationic form [65]. The lower pH facilitate corrosion of the zerovalent metal into metal ions which facilitate catalyzation of $S_2O_8^{2-}$ into $^{\bullet}OH$ and $SO_4^{\bullet-}$ [29,63]. Other possibilities of the high removal of CFA at pH < 8.2 might be the positively charged surface of the catalyst which adhere maximum accumulation of negatively charged $S_2O_8^{2-}$ and possibly led to high yield of $^{\bullet}OH$ and $SO_4^{\bullet-}$ [62,66]. At very high pH (pH = 10.6), the slower degradation of CFA looked to be due to: (a suppress corrosion of Bi/Cu^0; (b formation of hydroxide complexes of the zerovalent metal; and (c scavenging of $^{\bullet}OH$ and $SO_4^{\bullet-}$ by ^{-}OH [63,65,67].

Impact of inorganic ions: Inorganic ions are ubiquitous in water and some believed to exhibit high reaction rate with $^{\bullet}OH$ and $SO_4^{\bullet-}$. Thus, addition of these ions into aqueous CFA solution could lower reactivities of $^{\bullet}OH$ and $SO_4^{\bullet-}$ with the target contaminant [29,68]. To check the consequences of inorganic ions, the removal of CFA by Bi/Cu^0-catalyzed $S_2O_8^{2-}$ was studied in the presence of some inorganic anions, e.g., NO_2^-, CO_3^{2-}, HCO_3^-, and NO_3^- and inorganic cations, e.g., Cu^+, Fe^{3+}, Fe^{2+}, Zn^{2+}, and Mn^{2+}. Fig. 7c display the effects of inorganic anions which illustrate greater degree of inhibition by NO_2^- followed by CO_3^{2-} and HCO_3^- while NO_3^- exhibited insignificant influence. Among the mentioned inorganic anions, NO_2^- as shown in reactions (20) and (21) demonstrate faster kinetics with $^{\bullet}OH$ and $SO_4^{\bullet-}$ and consequently impede highly the reactivities of the reactive radicals with CFA molecules [68,69]. The CO_3^{2-} and HCO_3^- also exhibit high kinetics with $^{\bullet}OH$ and $SO_4^{\bullet-}$ as presented in reactions (22) to (25) and consequently led to low degree of CFA removal [68,69]. Among the inorganic anions, the low degree of inhibition by NO_3^- could be because of the smaller reactivity between NO_3^- and $SO_4^{\bullet-}$ as shown in reaction (26).

Additionally, the inorganic anions with negative charge could hinder accumulation of the negatively charged $S_2O_8^{2-}$ on the surface of the catalyst and consequently retard removal efficiency of CFA.

$$\bullet OH + NO_2^- \rightarrow {}^-OH + NO_2^{\bullet} \quad (k_{20} = 8.0 \times 10^9\ M^{-1}s^{-1}) \tag{20}$$

$$SO_4^{\bullet-} + NO_2^- \rightarrow SO_4^{2-} + NO_2^{\bullet} \quad (k_{21} = 8.8 \times 10^8\ M^{-1}s^{-1}) \tag{21}$$

$$\bullet OH + CO_3^{2-} \rightarrow {}^-OH + CO_3^{\bullet-} \quad (k_{22} = 4.0 \times 10^8\ M^{-1}s^{-1}) \tag{22}$$

$$SO_4^{\bullet-} + CO_3^{2-} \rightarrow SO_4^{2-} + CO_3^{\bullet-} \quad (k_{23} = 4.1 \times 10^6\ M^{-1}s^{-1}) \tag{23}$$

$$\bullet OH + HCO_3^- \rightarrow CO_3^{\bullet-} + H_2O \quad (k_{24} = 8.5 \times 10^6\ M^{-1}s^{-1}) \tag{24}$$

$$SO_4^{\bullet-} + HCO_3^- \rightarrow SO_4^{2-} + CO_3^{\bullet-} + H^+ \quad (k_{25} = 3.5 \times 10^6\ M^{-1}s^{-1}) \tag{25}$$

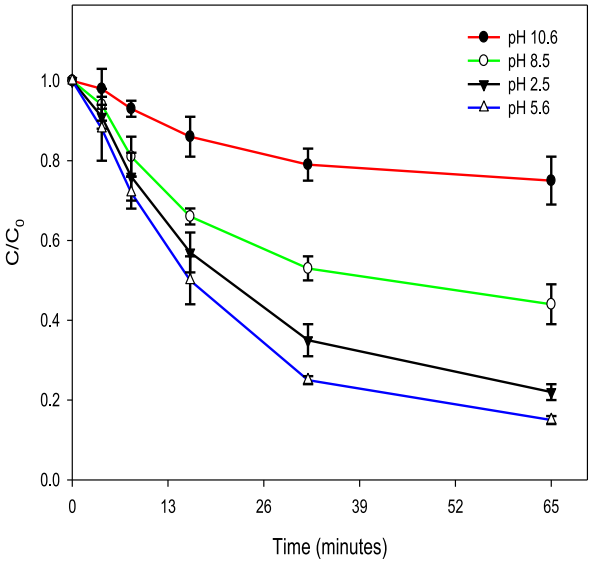

Fig. 7b. Impacts of pH on the treatment of CFA by $Bi/Cu^0/S_2O_8^{2-}$. $[CFA]_0 = 10$ mg/L, $[S_2O_8^{2-}]_0 = 40$ mg/L, $[Bi/Cu^0] = 0.5$ g/L, pH = 2.5 to 10.6.

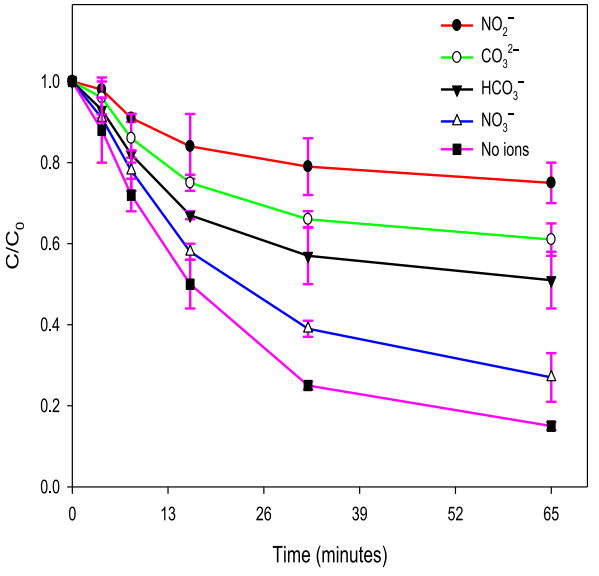

Fig. 7c. Impacts of inorganic anions on the treatment of CFA by $Bi/Cu^0/S_2O_8^{2-}$. $[CFA]_0 = 10$ mg/L, $[S_2O_8^{2-}]_0 = 40$ mg/L, $[Bi/Cu^0] = 0.5$ g/L, $[NO_2^-$, CO_3^{2-}, HCO_3^-, and $NO_3^-] = 100$ mg/L, pH = 5.6 (pH was 8.7 in the case of CO_3^{2-} and HCO_3^-).

$$SO_4^{\bullet-} + NO_3^- \rightarrow SO_4^{2-} + NO_3^{\bullet} + \left(k_{26} = 5.0 \times 10^4\ M^{-1}s^{-1}\right) \quad (26)$$

The inorganic cations, Cu^+, Fe^{3+}, Fe^{2+}, Zn^{2+}, and Mn^{2+} were added individually into the CFA solution and treated with Bi/Cu^0-catalyzed $S_2O_8^{2-}$. The results in Fig. 7d illustrate that cations Fe^{2+}, Zn^{2+}, and Mn^{2+} showed more pronounced effect on the degradation of CFA than Cu^+ and Fe^{3+}. It is shown that transition metals catalyze $S_2O_8^{2-}$ into $^{\bullet}OH$ and $SO_4^{\bullet-}$ [70,71]. The additional activation of $S_2O_8^-$ by these metals in addition to Bi/Cu^0 could be the possible reason for the enhanced removal of CFA. Due to positive charge, these metals facilitate binding and accumulation of negatively charged $S_2O_8^{2-}$ on the surface of Bi/Cu^0 and could promote the yield of reactive radicals. The smaller facilitation by Cu + looked to be due to its greater scavenging of reactive $^{\bullet}OH$ as shown in reaction (27) [68]. The Fe^{3+} is reported to yield less reactive radical from the activated $S_2O_8^{2-}$ and might be the cause of its less facilitation of CFA degradation [71].

$$\bullet OH + Cu^+ \rightarrow {}^-OH + Cu^{2+}\ \left(k_{27} = 3.0 \times 10^9\ M^{-1}s^{-1}\right) \quad (27)$$

Impacts of temperature: The increasing temperature is reported to promote the degree of degradation of target pollutants [5,72,

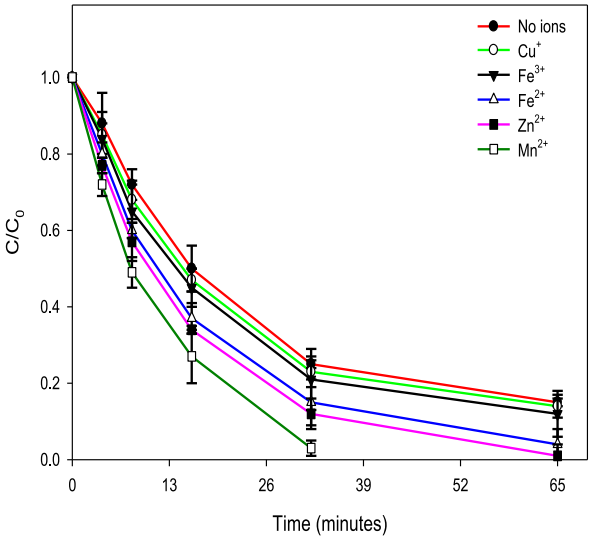

Fig. 7d. Impacts of inorganic cations on the treatment of CFA by $Bi/Cu^0/S_2O_8^{2-}$. $[CFA]_0 = 10$ mg/L, $[S_2O_8^{2-}]_0 = 40$ mg/L, $[Bi/Cu^0] = 0.5$ g/L, [Cu^+, Fe^{2+}, Fe^{3+}, Zn^{2+}, Mn^{2+}] = 100 mg/L, pH = 5.6.

73]. Thus, degradation of CFA by Bi/Cu^0-catalyzed $S_2O_8^{2-}$ was analyzed at four different temperatures, i.e., 298, 303, 313, and 323 K. The results achieved (Fig. 7e) showed promising effects of temperature on the degree of degradation of CFA. The rise in temperature was found to shorten treatment time and at 32 min time, the use of $Bi/Cu^0/S_2O_8^{2-}$ resulted into 75, 82, 92, and 98% removal efficiency of CFA at 298, 303, 313, and 323 K, respectively (Fig. 7e). The rise in temperature reportedly lowered the reaction activation energy which subsequently led to faster collision between Bi/Cu^0 and $S_2O_8^{2-}$ and promote the yield of reactive radicals [73]. The lower activation energy with increasing temperature could result into more molecules of CFA to cross the energy barrier and react with reactive radicals as well as accumulate on the surface of the catalyst [73].

The degradation of CFA at different temperatures was investigated by different kinetic models and found to best fit *pseudo-first-order*. The *k* values obtained were significantly increased from 0.003 to 0.012 min^{-1} with elevating temperature from 298 to 323 K. The prompt activation of $S_2O_8^{2-}$, rapid rate of $^{\bullet}OH$ and $SO_4^{\bullet-}$ formation, and consequently more collision of $^{\bullet}OH$ and $SO_4^{\bullet-}$ with CFA molecules looked to be the possibility of increasing *k* values with elevating temperature [73]. The values of –ln *k* versus $\frac{1}{T}$ from Arrhenius equation (equation (10)) were plotted and showed linear relationship with $R^2 = 0.99$. The plot of –ln *k* versus $\frac{1}{T}$ was used to calculate the activation energy (Ea) of the degradation of CFA which come out to be 45. 5 kJ/mol. This value of Ea was used to calculate enthalpy, ΔH of CFA removal by the Bi/Cu^0-catalyzed $S_2O_8^{2-}$ process at different temperatures used. The values of ΔH at 298, 303, 313, and 323 K were obtained as 43.1, 43.0, 42.9, and 42.8 kJ/mol, respectively.

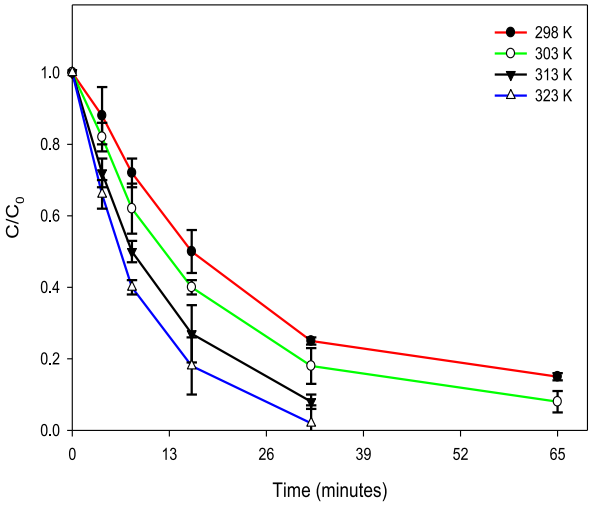

Fig. 7e. Impacts of temperature on the treatment of CFA by $Bi/Cu^0/S_2O_8^{2-}$. $[CFA]_0 = 10$ mg/L, $[S_2O_8^{2-}]_0 = 40$ mg/L, $[Bi/Cu^0] = 0.5$ g/L Temperature = 298, 303, 313, and 323 K, pH = 5.6.

3.7. Treatment of CFA in real water samples

The Cu^0-and Bi/Cu^0-catalyzed $S_2O_8^{2-}$ processes were used to treat CFA in real water samples, Sample 1 and Sample 2 collected from two different location in District Vehari, Pakistan. The Sample 1 and Sample 2 characteristics are presented in our previous published work [28]. The results obtained from the treatment of CFA in Sample 1 and Sample 2 were compared with that in deionized water (DIW) and shown in Fig. 8. The Cu^0-catalyzed $S_2O_8^{2-}$ process gave CFA removal efficiency of 52, 47, and 67% in Sample 1, Sample 2, and DIW, respectively, at 65 min. The removal efficiency of CFA caused by the Bi/Cu^0-catalyzed $S_2O_8^{2-}$ process in Sample 1, Sample 2, and DIW was 72, 64, and 85%, respectively, at 65 min. These results illustrate high potential of both Cu^0-catalyzed $S_2O_8^{2-}$ and Bi/Cu^0-catalyzed $S_2O_8^{2-}$ processes in the treatment of CFA in real water samples. Since the collected real water samples contain both cations and anions, the anions scavenge reactive radicals and at the same time, cations facilitate activation of $S_2O_8^{2-}$ into reactive radicals. The study is helpful to extend applications of the Cu^0 and Bi/Cu^0 in treatment of CFA and other organic pollutants in real water.

3.8. Ecotoxicity assessment studies

The identification of the ecotoxicities level of CFA and its degradation products were determined to evaluate potential and greenness of the Cu^0-and Bi/Cu^0-catalyzed $S_2O_8^{2-}$ processes. The acute and/or chronic toxicities of CFA and its products were determined at three levels of aquatic organisms, i.e., fish, green algae and daphnia following the criteria discussed in our previous published studies [29,74]. The results from the ecotoxicities evaluation are given in Table 2 which illustrates low toxicities level of the CFA and its two products (2-(4-hydroxyphenoxy)-isobutyric acid and hydroquinone) towards all aquatic organisms. The products, 4-chlorophenol and chlorobenzene showed harmful effects at all levels. The hydroquinone which proved to be non-toxic is reported to be degraded into further non-toxic smaller fragments, e.g., acetate. The harmful products evolved from the treatment of emerging pollutants provide bases for future studies to consider toxicities of degradation products along with parent compound.

3.9. Comparison of Bi/Cu^0 efficiency

The performance of the prepared material, Bi/Cu^0 used in the present study for activation of $S_2O_8^{2-}$ and degradation of CFA was compared with other catalyzed-$S_2O_8^{2-}$ processes for treatment of other organic pollutants. The comparative efficiency of different processes with detailed experimental conditions is given in Table 3. The results illustrate that Bi/Cu^0 exhibit significantly high performance in the treatment of CFA at a lower dose of $S_2O_8^{2-}$ and treatment time.

4. Conclusions

The Bi coupling showed fruitful results and effectively enhanced the structural characteristics, stability, and catalytic activity of Cu^0. The Bi/Cu^0 proved to effectively decompose $S_2O_8^{2-}$ and showed high reusability, leading to 59% degradation of CFA at six cycles of treatment as compared to 85% at first cycle. The Bi/Cu^0/$S_2O_8^{2-}$ proved to be effective intreating high concentration of CFA and led to 63% removal of 20 mg/L CFA versus 85% of 10 mg/L CFA. The Bi/Cu^0/$S_2O_8^{2-}$ was effective in treating CFA in real water samples, in the presence of counter ions and at different pH. The use of high temperature (323 K), high concentration of Bi/Cu^0 (1.0 g/L), and high

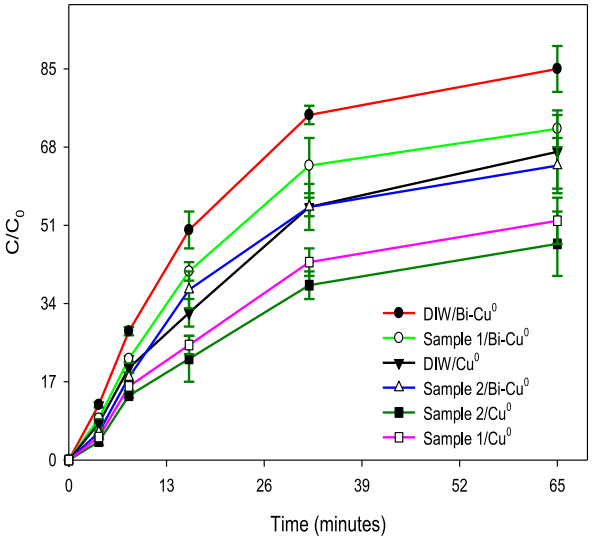

Fig. 8. Treatment of CFA by Cu^0/$S_2O_8^{2-}$ and Bi/Cu^0/$S_2O_8^{2-}$ in real water samples. $[CFA]_0 = 10$ mg/L, $[S_2O_8^{2-}]_0 = 40$ mg/L, $[Bi/Cu^0] = 0.5$ g/L.

Table 2
Analysis of ecotoxicities of CFA and its products in the units of mg/L*.

Compound	Fish (LC_{50})	Daphnia (LC_{50})	Green Algae (EC_{50})	Fish (ChV)	Daphnia (ChV)	Green Algae (ChV)
Clofibric acid	307.9	189.03	194.3	33.0	22.8	60.5
2-(4-hydroxyphenoxy)-isobutyric acid	557.2	148.04	699.7	53.9	28.1	329.9
Chlorobenzene	24.7	14.9	14.1	2.6	1.7	4.2
4-chlorophenol	76.2	43.9	34.7	7.5	4.4	9.4
Hydroquinone	668.7	347.2	178.8	58.8	26.4	38.3

*Acute toxicities were determined using European Union guidelines (Annex VI/Directive 67/548/EEC), i.e., LC_{50} and $EC_{50} > 100$ (Not harmful), $100 > LC_{50} > 10$ or $100 > EC_{50} > 10$ (Harmful), $10 > LC_{50} > 1$ or $10 > EC_{50} > 1$ (Toxic), EC_{50} and $LC_{50} < 1$ (Very toxic). Chronic toxicities were estimated using Chinese guidelines for new hazard chemical substances (HJ/T154–2004), e.g., ChV>10 (Not harmful), 10 > ChV >1 (Harmful), 1 > ChV>0.1 (Toxic), and ChV<0.1 (Very toxic).

Table 3
Comparative study of the efficiency of Bi/Cu^0-cattalyzed $S_2O_8^{2-}$ process with other catalyzed $S_2O_8^{2-}$based processes.

$[Catalyst]_0$ mg/L	$[Pollutant]_0$ mg/L	pH	$[S_2O_8^{2-}]_0$ mg/L	%Removal efficiency/time	Reference
MMBC = 200	TC = 20	3.0	1536	93/180 min	[27]
MRSB = 1000	TCH = 20	5.68	1536	98/120 min	[75]
PVP-nZVI-Cu = 400	TCE = 20	6.5	1152	99.5/60 min	[76]
MNP = 300	NOR = 5	4.0	960	90/60 min	[26]
nZVCe/PB = 200	NOR = 10	6.7	80	84/70 min	[28]
ZVCu = 500	BFAF = 6.7	4.0	192	60/60 min	[77]
Bi/Cu^0 = 500	CFA	5.6	40	85/65	Present work

dose of $S_2O_8^{2-}$ (80 mg/L) caused 100%, 99.5, and 99% removal of CFA, respectively, at 65 min. The use of cations scavengers facilitated efficiency of $Bi/Cu^0/S_2O_8^{2-}$ while anions inhibited its efficiency. The different scavenging experiments revealed that $^{\bullet}OH$ and $SO_4^{\bullet-}$ were formed in the catalyzed $S_2O_8^{2-}$-based process and reacted fast with CFA. The increasing concentrations of IPA and TBA greatly restrained removal of CFA. The low leaching of Cu ions (0.12 mg/L) from Bi/Cu^0 at sixth cycle suggest its high fruitfulness and environmentally friendly nature. The degradation products analysis revealed the formation of different $^{\bullet}OH$ and $SO_4^{\bullet-}$-based products of CFA whose toxicities were evaluated and found the final product hydroquinone as non-toxic.

Declaration of generative AI in scientific writing

During the preparation of this work the author(s) did not use AI and AI-assisted technologies in writing process.

Authorship contribution

1. **Jibran Iqbal**: Funding acquisition, Methodology, Analysis, and Writing original draft.
2. **Noor S. Shah**: Resources, Supervision, writing original draft.
3. **Javed Ali Khan**: Data Visualization, Analysis.
4. **Mohamed A. Habila**: Review & Editing, Funding acquisition.
5. **Grzegorz Boczkaj**: Writing - Review & Editing.
6. **Asam Shad**: Analysis, Review & Editing.
7. **Yousef Nazzal**: Data visualization, Analysis.
8. **Ahmed A. Al-Taani**: Data visualization, Analysis.
9. **Fares Howari**: Data visualization, Review & Editing.

Declaration of competing interest

The authors declare that they have no known competing financial interests or personal relationships that could have appeared to influence the work reported in this paper.

Data availability

Data will be made available on request.

Acknowledgement

The study was supported by Zayed University, Abu Dhabi, UAE under the RIF Grant R22166 (**to Jibran Iqbal**). The authors also thank the Researchers Supporting Project number (RSP2023R441), King Saud University, Riyadh, Saudi Arabia for the financial

support.

References

[1] J. Barasarathi, P.S. Abdullah, E.C. Uche, Application of magnetic carbon nanocomposite from agro-waste for the removal of pollutants from water and wastewater, Chemosphere 305 (2022), 135384.

[2] J. Iqbal, N.S. Shah, M. Sayed, N.K. Niazi, M. Imran, J.A. Khan, Z.U.H. Khan, A.G.S. Hussien, K. Polychronopoulou, F. Howari, Nano-zerovalent manganese/biochar composite for the adsorptive and oxidative removal of Congo- red dye from aqueous solutions, J. Hazard Mater. 403 (2021), 123854.

[3] M. Imran, B. Murtaza, S. Ansar, N.S. Shah, Z.U.H. Khan, S. Ali, G. Boczkaj, F. Hafeez, S. Ali, M. Rizwan, Potential of nanocomposites of zero valent copper and magnetite with Eleocharis dulcis biochar for packed column and batch scale removal of Congo red dye, Environ. Pollut. 305 (2022), 119291.

[4] F.A. Janjhi, I. Ihsanullah, M. Bilal, R. Castro-Muñoz, G. Boczkaj, F. Gallucci, MXene-based materials for removal of antibiotics and heavy metals from wastewater–a review, Water Resour. Ind. 29 (2023), 100202.

[5] I. Maamoun, O. Falyouna, R. Eljamal, K. Bensaida, K. Tanaka, T. Tosco, Y. Sugihara, O. Eljamal, Multi-functional magnesium hydroxide coating for iron Nanoparticles towards prolonged reactivity in Cr (VI) removal from aqueous solutions, J. Environ. Chem. Eng. 10 (2022), 107431.

[6] D.N. Ahmed, L.A. Naji, A.A.H. Faisal, N. Al-Ansari, M. Naushad, Waste foundry sand/MgFe-layered double hydroxides composite material for efficient removal of Congo red dye from aqueous solution, Sci. Rep. 10 (2020) 2042.

[7] K. Balasubramani, N. Sivarajasekar, M. Naushad, Effective adsorption of antidiabetic pharmaceutical (metformin) from aqueous medium using graphene oxide nanoparticles: equilibrium and statistical modelling, J. Mol. Liq. 301 (2020), 112426.

[8] J. Iqbal, N.S. Shah, M. Sayed, N. Muhammad, S.-u. Rehman, J.A. Khan, Z.U.H. Khan, F.M. Howari, Y. Nazzal, C. Xavier, S. Arshad, A. Hussein, K. Polychronopoulou, Deep eutectic solvent-mediated synthesis of ceria nanoparticles with the enhanced yield for photocatalytic degradation of flumequine under UV-C, J. Water Process Eng. 33 (2020), 101012.

[9] S. Muthusaravanan, N. Sivarajasekar, J.S. Vivek, T. Paramasivan, M. Naushad, J. Prakashmaran, V. Gayathri, O.K. Al-Duaij, Phytoremediation of Heavy Metals: Mechanisms, Methods and Enhancements, Environmental Chemistry Letters, 2018, pp. 1339–1359.

[10] M. Naushad, Surfactant assisted nano-composite cation exchanger: development, characterization and applications for the removal of toxic Pb^{2+} from aqueous medium, Chem. Eng. J. 235 (2014) 100–108.

[11] N.S. Shah, J. Iqbal, M. Sayed, A.A. Ghfar, J.A. Khan, Z.U.H. Khan, B. Murtaza, G. Boczkaj, F. Jamil, Enhanced solar light photocatalytic performance of Fe-ZnO in the presence of H_2O_2, $S_2O_8^{2-}$, and HSO_5^- for degradation of chlorpyrifos from agricultural wastes: toxicities investigation, Chemosphere 287 (2022), 132331.

[12] T. Shubair, O. Eljamal, A. Khalil, N. Matsunaga, Nitrate removal in porous media using nanoscale zero valent iron: column experiment, in: Proceedings of International Exchange and Innovation Conference on Engineering & Sciences (IEICES), 2017, https://doi.org/10.15017/1906408.

[13] O. Falyouna, K. Bensaida, I. Maamoun, U.P.M. Ashik, A. Tahara, K. Tanaka, N. Aoyagi, Y. Sugihara, O. Eljamal, Synthesis of hybrid magnesium hydroxide/magnesium oxide nanorods [Mg (OH) 2/MgO] for prompt and efficient adsorption of ciprofloxacin from aqueous solutions, J. Clean. Prod. 342 (2022), 130949.

[14] O. Falyouna, M.F. Idham, I. Maamoun, K. Bensaida, U.P.M. Ashik, Y. Sugihara, O. Eljamal, Promotion of ciprofloxacin adsorption from contaminated solutions by oxalate modified nanoscale zerovalent iron particles, J. Mol. Liq. 359 (2022), 119323.

[15] Z. Honarmandrad, X. Sun, Z. Wang, M. Naushad, G. Boczkaj, Activated persulfate and peroxymonosulfate based advanced oxidation processes (AOPs) for antibiotics degradation–A review, Water Resour. Ind. 29 (2022), 100194.

[16] J. Iqbal, N.S. Shah, M. Sayed, J.A. Khan, M. Imran, Z.U.H. Khan, N.K. Niazi, A.A. Al- Taani, F. Howari, Y. Nazzal, Exploring the potential of nano- zerovalent copper modified biochar for the removal of ciprofloxacin from water, Environ. Nanotechnol. Monit. Manag. 16 (2021), 100604.

[17] H. Lin, X. Zhong, C. Ciotonea, X. Fan, X. Mao, Y. Li, B. Deng, H. Zhang, S. Royer, Efficient degradation of clofibric acid by electro-enhanced peroxydisulfate activation with Fe-Cu/SBA-15 catalyst, Appl. Catal. B Environ. 230 (2018) 1–10.

[18] I. Sirés, E. Brillas, Remediation of water pollution caused by pharmaceutical residues based on electrochemical separation and degradation technologies: a review, Environ. Int. 40 (2012) 212–229.

[19] X. Yang, R.C. Flowers, H.S. Weinberg, P.C. Singer, Occurrence and removal of pharmaceuticals and personal care products (PPCPs) in an advanced wastewater reclamation plant, Water Res. 45 (2011) 5218–5228.

[20] X.J. Kong, Z.H. Wu, Z.R. Ren, K.H. Guo, S.D. Hou, Z.C. Hua, X.C. Li, J.Y. Fang, Degradation of lipid regulators by the UV/chlorine process: radical mechanisms, chlorine oxide radical (ClO•)- mediated transformation pathways and toxicity changes, Water, Research 137 (2018) 242–250.

[21] H. Lin, J. Wu, H. Zhang, Degradation of clofibric acid in aqueous solution by an EC/Fe^{3+}/PMS process, Chem. Eng. J. 244 (2014) 514–521.

[22] K. Zhu, X. Wang, M. Geng, D. Chen, H. Lin, H. Zhang, Catalytic oxidation of clofibric acid by peroxydisulfate activated with wood-based biochar: effect of biochar pyrolysis temperature, performance and mechanism, Chem. Eng. J. 374 (2019) 1253–1263.

[23] X. Lu, Y.S. Shao, N.Y. Gao, J.X. Chen, H.P. Deng, W.H. Chu, N. An, F.Y. Peng, Investigation of clofibric acid removal by UV/persulfate and UV/chlorine processes: kinetics and formation of disinfection byproducts during subsequent chlor(am)ination, Chem. Eng. J. 331 (2018) 364–371, 2018.

[24] C. Cai, X. Duan, X. Xie, S. Kang, C. Liao, J. Dong, Y. Liu, S. Xiang, D.D. Dionysiou, Efficient degradation of clofibric acid by heterogeneous catalytic ozonation using $CoFe_2O_4$ catalyst in water, J. Hazard Mater. 410 (2021), 124604.

[25] S.S. Sable, S.C. Panchangam, S.L. Lo, Abatement of clofibric acid by Fenton-like process using iron oxide supported sulfonated-ZrO_2: efficient heterogeneous catalysts, J. Water Process Eng. 26 (2018) 92–99.

[26] D.H. Ding, C. Liu, Y.F. Ji, Q. Yang, L.L. Chen, C.L. Jiang, T.M. Cai, Mechanism insight of degradation of norfloxacin by magnetite nanoparticles activated persulfate: identification of radicals and degradation pathway, Chem. Eng. J. 308 (2017) 330–339.

[27] D.L. Huang, Q. Zhang, C. Zhang, R.Z. Wang, R. Deng, H. Luo, T. Li, J. Li, S. Chen, C.H. Liu, Mn doped magnetic biochar as persulfate activator for the degradation of tetracycline, Chem. Eng. J. 391 (2020), 123532.

[28] J. Iqbal, N.S. Shah, M. Sayed, S. Rauf, Z.U.H. Khan, N.K. Niazi, K. Polychronopoulou, F. Howari, F. Rehman, Efficient removal of norfloxacin using nano zerovalent cerium composite biochar-catalyzed peroxydisulfate, J. Clean. Prod. 377 (2022), 134405.

[29] N.S. Shah, J.A. Khan, M. Sayed, Z.U.H. Khan, H.S. Ali, B. Murtaza, H.M. Khan, M. Imran, N. Muhammad, Hydroxyl and sulfate radical mediated degradation of ciprofloxacin using nano zerovalent manganese catalyzed S2O82, Chem. Eng. J. 356 (2019) 199–209.

[30] N.S. Shah, J.A. Khan, M. Sayed, Z.U.H. Khan, J. Iqbal, S. Arshad, M. Junaid, H.M. Khan, Synergistic effects of H_2O_2 and $S_2O_8^{2-}$ in the gamma radiation induced degradation of Congo-red dye: kinetics and toxicities evaluation, Sep. Purif. Technol. 233 (2020), 115966.

[31] C. Kim, J.Y. Ahn, T.Y. Kim, W.S. Shin, I. Hwang, Activation of persulfate by nanosized zero-valent iron (NZVI): mechanisms and transformation products of NZVI, Environ. Sci. Technol. 52 (2018) 3625–3633.

[32] Y. Wang, S.Y. Chen, X. Yang, X.F. Huang, Y.H. Yang, E.K. He, S. Wang, R.L. Qiu, Degradation of 2, 2′, 4, 4′-tetrabromodiphenyl ether (BDE-47) by a nano zerovalent iron-activated persulfate process: the effect of metal ions, Chem. Eng. J. 317 (2017) 613–622.

[33] M. Wang, Y. Wang, X. Jing, J. Xu, M. Li, Q. Xie, X. Cai, Developments of efficient dithionite-zerovalent iron/persulfate systems with accelerated Fe (III)/Fe (II) Cycle for PAHs removal in water and soils, Chem. Eng. J. 463 (2023), 142325.

[34] F. Rehman, N. Parveen, J. Iqbal, M. Sayed, N.S. Shah, S. Ansar, J.A. Khan, A. Shah, F. Jamil, G. Boczkaj, Potential degradation of norfloxacin using UV-C/Fe^{2+}/peroxides-based oxidative pathways, J. Photochem. Photobiol. Chem. 435 (2023), 114305.

[35] K. Bensaida, O. Falyouna, I. Maamoun, R. Eljamal, O. Eljamal, Enhancement of power generation in microbial fuel cells (MFCs) using iron/copper nanoparticles, in: Proceedings of International Exchange and Innovation Conference on Engineering & Sciences (IEICES), 2020, https://doi.org/10.5109/4102482.

[36] K. Bensaida, I. Maamoun, R. Eljamal, O. Falyouna, Y. Sugihara, O. Eljamal, New insight for electricity amplification in microbial fuel cells (MFCs) applying magnesium hydroxide coated iron nanoparticles, Energy Convers. Manag. 249 (2021), 114877.

[37] R. Eljamal, I. Maamoun, K. Bensaida, G. Yilmaz, Y. Sugihara, O. Eljamal, A novel method to improve methane generation from waste sludge using iron nanoparticles coated with magnesium hydroxide, Renew. Sustain. Energy Rev. 158 (2022), 112192.

[38] S. Kumar, P. Kaur, R.S. Brar, J.N. Babu, Nanoscale zerovalent copper (nZVC) catalyzed environmental remediation of organic and inorganic contaminants: a review, Heliyon 8 (2022), e10140.
[39] N.S. Shah, J.A. Khan, M. Sayed, J. Iqbal, Z.U.H. Khan, N. Muhammad, K. Polychronopoulou, S. Hussain, M. Imran, B. Murtaza, M. Usman, Nano-zerovalent copper as a Fenton-like catalyst for the degradation of ciprofloxacin in aqueous solution, J. Water Process Eng. 37 (2020), 101325.
[40] J. Gong, C.S. Lee, Y.Y. Chang, Y.S. Chang, Novel self-assembled bimetallic structure of Bi/Fe^0: the oxidative and reductive degradation of hexahydro-1, 3, 5-trinitro-1, 3, 5-triazine (RDX), J. Hazard Mater. 286 (2015) 107–117.
[41] B. Murtaza, N.S. Shah, M. Sayed, J.A. Khan, M. Imran, M. Shahid, Z.U.H. Khan, A. Ghani, G. Murtaza, N. Muhammad, M.S. Khalid, Synergistic Effects of bismuth coupling on the reactivity and reusability of zerovalent iron nanoparticles for the removal of cadmium from aqueous solution, Sci. Total Environ. 669 (2019) 333–341.
[42] M. Sayed, A. Khan, S. Rauf, N.S. Shah, F. Rehman, A.A. Al-Kahtani, J.A. Khan, J. Iqbal, G. Boczkaj, I. Gul, M. Bushra, Bismuth-doped nano zerovalent iron: a novel catalyst for chloramphenicol degradation and hydrogen production, ACS Omega 5 (2020) 30610–30624.
[43] C. Liang, C.F. Huang, N. Mohanty, R.M. Kurakalva, A rapid spectrophotometric determination of persulfate anion in ISCO, Chemosphere 73 (2008) 1540–1543.
[44] N.S. Shah, J.A. Khan, M. Sayed, Z.U.H. Khan, A.D. Rizwan, N. Muhammad, G. Boczkaj, B. Murtaza, M. Imran, H.M. Khan, G. Zaman, Solar Light driven degradation of norfloxacin using as-synthesized Bi^{3+} and Fe^{2+} co- doped ZnO with the addition of HSO_5^-: toxicities and degradation pathways investigation, Chem. Eng. J. 351 (2018) 841–855.
[45] F. He, Z. He, J. Xie, Y. Li, IR and Raman spectra properties of Bi_2O_3-ZnO- B_2O_3-BaO quaternary glass system, Am. J. Anal. Chem. 5 (2014) 1142.
[46] ECOSAR. http://www.epa.gov/oppt/newchems/tools/21ecosar.htm, 2014.
[47] Y. Gao, T. An, Y. Ji, G. Li, C. Zhao, Eco-toxicity and human estrogenic exposure risks from •OH-initiated photochemical transformation of four phthalates in water: a computational study, Environ. Pollut. 206 (2015) 510–517.
[48] A.O.H. Jones, N. Voulvoulis, J.N. Lester, Aquatic environmental assessment of the top 25 English prescription pharmaceuticals, Water Res. 36 (2002) 5013–5022.
[49] X. He, S.P. Mezyk, I. Michael, D. Fatta-Kassinos, D.D. Dionysiou, Degradation kinetics and mechanism of β-lactam antibiotics by the activation of H_2O_2 and $Na_2S_2O_8$ under UV-254 nm irradiation, J. Hazard Mater. 279 (2014) 375–383.
[50] I. Maamoun, K. Bensaida, R. Eljamal, O. Falyouna, K. Tanaka, T. Tosco, Y. Sugihara, O. Eljamal, Rapid and efficient chromium (VI) removal from aqueous solutions using nickel hydroxide nanoplates (nNiHs), J. Mol. Liq. 358 (2022), 119216.
[51] C. Han, J. Xie, X. Min, Efficient adsorption H_3AsO4 and Cr (VI) from strongly acidic solutions by La-Zr bimetallic MOFs: crystallinity role and mechanism, J. Environ. Chem. Eng. 10 (2022), 108982.
[52] Y. Ding, L. Fu, X. Peng, M. Lei, C. Wang, J. Jiang, Copper catalysts for radical and nonradical persulfate based advanced oxidation processes: certainties and uncertainties, Chem. Eng. J. 427 (2022), 131776.
[53] L. Fang, K. Liu, F. Li, W. Zeng, Z. Hong, L. Xu, Q. Shi, Y. Ma, New insights into stoichiometric efficiency and synergistic mechanism of persulfate activation by zero-valent bimetal (Iron/Copper) for organic pollutant degradation, J. Hazard Mater. 403 (2021), 123669.
[54] Q. Ji, J. Li, Z. Xiong, B. Lai, Enhanced reactivity of microscale Fe/Cu bimetallic particles (mFe/Cu) with persulfate (PS) for p-nitrophenol (PNP) removal in aqueous solution, Chemosphere 172 (2017) 10–20.
[55] X. Huo, P. Zhou, Y. Liu, F. Cheng, Y. Liu, X. Cheng, Y. Zhang, Q. Wang, Removal of contaminants by activating peroxymonosulfate (PMS) using zero valent iron (ZVI)-based bimetallic particles (ZVI/Cu, ZVI/Co, ZVI/Ni, and ZVI/Ag), RSC Adv. 10 (2020) 28232–28242.
[56] R. Cheng, C. Cheng, G.H. Liu, X. Zheng, G. Li, J. Li, Removing pentachlorophenol from water using a nanoscale zero-valent iron/H_2O_2 system, Chemosphere 141 (2015) 138–143.
[57] N.S. Shah, J.A. Khan, A.A.H. Al-Muhtaseb, M. Sayed, H.M. Khan, Gamma radiolytic decomposition of endosulfan in aerated solution: the role of carbonate radical, Environ. Sci. Pollut. Control Ser. 23 (2016) 12362–12371.
[58] T. Csay, G. Rácz, Á. Salik, E. Takács, L. Wojnárovits, Reactions of clofibric acid with oxidative and reductive radicals-Products, mechanisms, efficiency and toxic effects, Radiat. Phys. Chem. 102 (2014) 72–78.
[59] X. Sun, Y. Qin, W. Zhou, Degradation of amoxicillin from water by ultrasound-zero-valent iron activated sodium persulfate, Sep. Purif. Technol. 275 (2021), 119080.
[60] X. Yu, X. Jin, N. Wang, Y. Yu, X. Zhu, M. Chen, Y. Zhong, J. Sun, L. Zhu, Transformation of sulfamethoxazole by sulfidated nanoscale zerovalent iron activated persulfate: mechanism and risk assessment using environmental metabolomics, J. Hazard Mater. 428 (2022), 128244.
[61] N. Azizollahi, E. Taheri, M.M. Amin, A. Rahimi, A. Fatehizadeh, X. Sun, S. Manickam, Hydrodynamic cavitation coupled with zero-valent iron produces radical sulfate radicals by sulfite activation to degrade direct red 83, Ultrason. Sonochem. 95 (2023), 106350.
[62] M. Sayed, J.A. Khan, L.A. Shah, N.S. Shah, F. Shah, H.M. Khan, P. Zhang, H. Arandiyan, Solar light responsive poly(vinyl alcohol)-assisted hydrothermal synthesis of immobilized TiO_2/Ti film with the addition of peroxymonosulfate for photocatalytic degradation of ciprofloxacin in aqueous media: a mechanistic approach, J. Phys. Chem. C 122 (2018) 406–421.
[63] S.-Y. Oh, S.-G. Kang, P.C. Chiu, Degradation of 2,4- dinitrotoluene by persulfate activated with zero-valent iron, Sci. Total Environ. 408 (2010) 3464–3468.
[64] D. Collins, T. Luxton, N. Kumar, S. Shah, V.K. Walker, V. Shah, Assessing the impact of copper and zinc oxide nanoparticles on soil: a field study, PLoS One 7 (2012), e42663.
[65] X. Zhang, Z. Liu, Q. Kong, G. Liu, W. Lv, F. Li, X. Lin, Aquatic photodegradation of clofibric acid under simulated sunlight irradiation: kinetics and mechanism analysis, RSC Adv. 8 (2018) 27796–27804.
[66] C. Tan, N. Gao, Y. Deng, J. Deng, S. Zhou, J. Li, X. Xin, Radical induced degradation of acetaminophen with Fe_3O_4 magnetic nanoparticles as heterogeneous activator of peroxymonosulfate, J. Hazard Mater. 276 (2014) 452–460.
[67] J. Zhao, Y. Zhang, X. Quan, S. Chen, Enhanced oxidation of 4- chlorophenol using sulfate radicals generated from zero-valent iron and peroxydisulfate at ambient temperature, Sep. Purif. Technol. 71 (2010) 302–307.
[68] G.V. Buxton, G.L. Greenstock, W.P. Helman, A.B. Ross, Critical review of rate constants for reactions of hydrated electrons, hydrogen atoms and hydroxyl radicals (•OH/•O^-) in aqueous solution, J. Phys. Chem. Ref. Data 17 (1988) 513–780.
[69] N.S. Shah, X. He, H.M. Khan, J.A. Khan, K.E. O'Shea, D.L. Boccelli, D.D. Dionysiou, Efficient removal of endosulfan from aqueous solution by UV-C/peroxides: a comparative study, J. Hazard Mater. 263 (2013) 584–592.
[70] B. Liu, B. Huang, Z. Wang, L. Tang, C. Ji, C. Zhao, L. Feng, Y. Feng, Homogeneous/heterogeneous metal-catalyzed persulfate oxidation technology for organic pollutants elimination: a Review, J. Environ. Chem. Eng. 11 (2023), 109586.
[71] N.S. Shah, X. He, J.A. Khan, H.M. Khan, D.L. Boccelli, D.D. Dionysiou, Comparative studies of various iron-mediated oxidative systems for the photochemical degradation of endosulfan in aqueous solution, J. Photochem. Photobiol. Chem. 306 (2015) 80–86.
[72] O. Eljamal, I. Maamoun, S. Alkhudhayri, R. Eljamal, O. Falyouna, K. Tanaka, N. Kozai, Y. Sugihara, Insights into boron removal from water using Mg-Al- LDH: reaction parameters optimization & 3D-RSM modeling, J. Water Process Eng. 46 (2022), 102608.
[73] N.S. Shah, A.D. Rizwan, J.A. Khan, M. Sayed, Z.U.H. Khan, B. Murtaza, J. Iqbal, S.U. Din, M. Imran, M. Nadeem, H. Ala'a, Toxicities, kinetics and degradation pathways investigation of ciprofloxacin degradation using iron- mediated H_2O_2 based advanced oxidation processes, Process Saf. Environ. Protect. 117 (2018) 473–482.
[74] N.S. Shah, J.A. Khan, M. Sayed, Z.U.H. Khan, J. Iqbal, M. Imran, B. Murtaza, A. Zakir, K. Polychronopoulou, Nano zerovalent zinc catalyzed peroxymonosulfate based advanced oxidation technologies for treatment of chlorpyrifos in aqueous solution: a semi-pilot scale study, J. Clean. Prod. 246 (2020), 119032.

[75] H.X. Huang, T. Guo, K. Wang, Y. Li, G.K. Zhang, Efficient activation of persulfate by a magnetic recyclable rape straw biochar catalyst for the degradation of tetracycline hydrochloride in water, Sci. Total Environ. 758 (2021), 143957.
[76] A. Idrees, A. Shan, M. Ali, Z. Abbas, T. Shahzad, S. Hussain, F. Mahmood, U. Farooq, M. Danish, S. Lyu, Highly efficient degradation of trichloroethylene in groundwater based on persulfate activation by polyvinylpyrrolidone functionalized Fe/Cu bimetallic nanoparticles, J. Environ. Chem. Eng. 9 (2021), 105341.
[77] Q. Wang, Y. Cao, H. Zeng, Y. Liang, J. Ma, X. Lu, Ultrasound-enhanced zero-valent copper activation of persulfate for the degradation of bisphenol AF, Chem. Eng. J. 378 (2019), 122143.